Cysteine Modification of a Putative Pore Residue in ClC-0
Implication for the Pore Stoichiometry of ClC Chloride Channels

Chia-Wei Lin and Tsung-Yu Chen

From the Department of Physiology, National Yang-Ming University, Taipei, Taiwan 11221

ABSTRACT The ClC channel family consists of chloride channels important for various physiological functions. Two members in this family, ClC-0 and ClC-1, share ~50–60% amino acid identity and show similar gating behaviors. Although they both contain two subunits, the number of pores present in the homodimeric channel is controversial. The double-barrel model proposed for ClC-0 was recently challenged by a one-pore model partly based on experiments with ClC-1 exploiting cysteine mutagenesis followed by modification with methanethiosulfonate (MTS) reagents. To investigate the pore stoichiometry of ClC-0 more rigorously, we applied a similar strategy of MTS modification in an inactivation-suppressed mutant (C212S) of ClC-0. Mutation of lysine 165 to cysteine (K165C) rendered the channel nonfunctional, but modification of the introduced cysteine by 2-aminoethyl MTS (MTSEA) recovered functional channels with altered properties of gating-permeation coupling. The fast gate of the MTSEA-modified K165C homodimer responded to external Cl^- less effectively, so the P_o-V curve was shifted to a more depolarized potential by ~45 mV. The K165C-K165 heterodimer showed double-barrel–like channel activity after MTSEA modification, with the fast-gating behaviors mimicking a combination of those of the mutant and the wild-type pore, as expected for the two-pore model. Without MTSEA modification, the heterodimer showed only one pore, and was easier to inactivate than the two-pore channel. These results showed that K165 is important for both the fast and slow gating of ClC-0. Therefore, the effects of MTS reagents on channel gating need to be carefully considered when interpreting the apparent modification rate.

KEY WORDS: chloride channel • ClC-0 • 2-aminoethyl methanethiosulfonate • double barrel

INTRODUCTION

ClC chloride channels play important roles in many physiological processes, including the control of cellular excitability, secretion of epithelial cells, and cell volume regulation (Pusch and Jentsch, 1994; Foskett, 1998; Jentsch et al., 1999; Valverde, 1999; Maduke et al., 2000). ClC-0 (Jentsch et al., 1990) and ClC-1 (Steinmeyer et al., 1991) are "muscle-type" chloride channels that, respectively, regulate the membrane potentials of the *Torpedo* electroplax and mammalian skeletal muscle cells. These two channels share ~50–60% amino acid sequence identity and biochemical studies have indicated that each is a homodimer (Middleton et al., 1994; Fahlke et al., 1997a) of a protein subunit with 10–12 putative transmembrane segments. Although they share the highest degree of homology in the ClC family (Jentsch et al., 1999), and also have similar electrophysiological behavior, one fundamental property of these two channels, the number of pores, is controversial.

In ClC-0, early electrophysiological studies suggested that a functional channel contains two identical pores. This double-barrel model was first proposed based on the single-channel recording trace, in which the active channel displays three current levels D (down, zero-current level), M (middle), and U (upper), likely corresponding to the opening of zero, one, and two pores, respectively. The argument was supported by the equally spaced current levels and a binomial distribution of their probabilities, which were seen across all tested membrane potentials and under diverse ionic conditions (Miller, 1982; Hanke and Miller, 1983; Miller and White, 1984; Bauer et al., 1991; Chen and Miller, 1996). Recently, experiments using genetic engineering techniques also showed that the two open substates (that is, the M and U levels) can be independently manipulated, and the conductance and gating behaviors of the pores are independent of one another (Middleton et al., 1996; Ludewig et al., 1996, 1997). It was therefore concluded that the two subunits of ClC-0 assemble to form two ion-conducting pathways in parallel and there is an axis of twofold symmetry between the two protopores.

On the other hand, the pore stoichiometry of ClC-1 was more difficult to address owing to a small single-channel conductance (Pusch et al., 1994; Saviane et al., 1999). Fahlke et al. (1998) recently proposed that the channel contains only one pore. An important line of evidence supporting this argument involved meth-

Address correspondence to Dr. Tsung-Yu Chen, Department of Physiology, National Yang-Ming University, 155, Section 2, Li-Nung Street, Taipei, Taiwan, 11221. Fax: 886-2-2826-4049; E-mail: tychen@ym.edu.tw

anethiosulfonate (MTS)[1] inhibition of cysteine-substituted channels, with particular attention to the behavior of homo- vs. heterodimers (Fahlke et al., 1997b, 1998). For example, the K231C homodimer was inhibited by externally applied MTS reagents at rates ~20-fold higher than was the single-cysteine heterodimer K231C-K231A. Assuming that MTS inhibition arises from pore occlusion, this result was considered as inconsistent with the two-pore model. Together with the inhibition of the various cysteine mutants by externally applied Cu^{2+}-phenanthroline and by internally applied cadmium ions, these results were used to argue that ClC-1 contains only one pore (Fahlke et al., 1998).

This apparent difference of pore stoichiometry between ClC-0 and ClC-1 is important because the biochemical components of these two channels are very similar. The controversy is even more intriguing after the demonstration of double-barrel–like single-channel activity in ClC-1 (Saviane et al., 1999). Given the molecular similarity of ClC-0 and ClC-1, how can one then reconcile these two fundamentally different pictures? There are several possibilities. First, ClC-0 and ClC-1 could contain only one pore and the characteristic double-barrel–like single-channel behavior found in these two channels may have another explanation (Fahlke et al., 1998). Alternatively, two separate pores may exist only on the intracellular side (Middleton et al., 1996) and the two ion-conducting pathways may merge as one pore to form the outer channel vestibule at the K165 position in ClC-0 (corresponding to K231 in ClC-1). Finally, because the ion permeation in both channels is coupled to the gating processes (Richard and Miller, 1990; Pusch et al., 1995; Chen and Miller, 1996; Rychkov et al., 1998), it is possible that the channels indeed have two separate pores and the apparent difference in MTS inhibition rates between the homo- and heterodimer in ClC-1 is due to an effect on the channel gating (Saviane et al., 1999). To clarify the pore stoichiometry of ClC channels, we adopt the same strategy (Fahlke et al., 1998) of modification with MTS reagents (Akabas et al., 1992; Stauffer and Karlin, 1994) on the introduced cysteine at the 165 position in ClC-0. We study the properties of the 2-aminoethyl MTS (MTSEA)–modified K165C homodimer and K165C-K165 heterodimer in detail. The MTSEA modification rates in these two channels are also compared.

MATERIALS AND METHODS

Mutagenesis and Channel Expression

Site-specific mutants were generated using PCR techniques, and all the PCR-generated regions were sequenced to exclude polymerase-induced errors. Wild-type ClC-0 and all mutants were constructed in pBluescript (Stratagene). Tandem dimers were constructed by linking two monomers with four residues (GTTS). Homodimeric channels were expressed by injecting oocytes with RNAs from monomeric constructs. Synthesis of RNAs and injection of *Xenopus* oocytes were done according to previously described methods (Chen, 1998; Lin et al., 1999). The injected oocytes were incubated in a high Ca^{2+}-ND96 solution containing (mM): 96 NaCl, 2 KCl, 1 $MgCl_2$, 1.8 $CaCl_2$, 5 HEPES, pH 7.6, containing 2–5 mM β-mercaptoethanol (β-ME; Bio-Rad Laboratories). For electrophysiological recording, β-ME was removed by transferring the oocytes to a fresh medium.

Macroscopic Current Recordings

Whole oocyte currents were measured using two-electrode voltage-clamp techniques. The standard bath (extracellular) solution was ND96 solution containing (mM): 96 NaCl, 2 KCl, 1 $MgCl_2$, 0.3 $CaCl_2$, 5 HEPES, pH 7.6. MTS reagents were purchased from Toronto Research Chemicals. Stock solutions of 0.1 M were prepared in distilled water and stored at −70°C. Working solutions containing the indicated concentrations of the MTS reagents were made immediately before use. To examine the MTSEA-induced current, the membrane potential of the oocyte was clamped at −30 mV, and the current was monitored with two types of repeated pulsing protocols: (a) a +40-mV voltage step for 50 ms, and (b) a +40-mV voltage step for 50 ms followed by a −150-mV voltage step for 100 ms. The voltage pulses were given at 0.1–1 Hz and the current was measured at the end of the +40-mV voltage step.

Examination of the fast-gate open probability (P_o) from macroscopic oocyte current followed the previously described voltage protocols (Chen, 1998; Lin et al., 1999). In brief, a positive voltage pulse (usually in the range of +40 to +120 mV) was given for 100 ms, followed by different test voltages from +120 to −160 mV in −20-mV steps. The tail current was measured at −100 mV and the extrapolated value to the beginning of the pulse was normalized to that obtained after the +120-mV test pulse. To examine the P_o-V curves in different Cl^- concentrations ($[Cl^-]$), solutions were (mM): X NaCl, (96-X) Naglutamate, 2 KCl, 1 $MgCl_2$, 0.3 $CaCl_2$, 5 HEPES, pH 7.6, giving the total $[Cl^-]$ of 4.6, 20, 60, 100.6, 150, 200, and 300 mM (when $[Cl^-] \geq 100.6$ mM, no Naglutamate was added). To make 1.6 mM $[Cl^-]$ solution, 1 mM KCl from the 4 mM $[Cl^-]$ solution was removed and $MgCl_2$ was replaced by $MgSO_4$. The opening rate α of the fast gate was calculated from the equation $\alpha = P_o/\tau$, in which τ was the time constant of the current relaxation at the membrane potential where P_o was obtained. Current block by SCN^- was examined by pulsing protocol 2, with the indicated concentrations of NaSCN being directly added to the bath ND96 solution. The anomalous mole fraction experiments were also performed with pulsing protocol 2 in solutions containing (mM): X NaCl, (100-X) NaSCN, 1 $MgSO_4$, 5 HEPES, pH 7.6, where NaSCN concentrations were 0, 3, 10, 20, 50, 80, and 100 mM, and the currents in different ionic mixtures were measured at +40 mV. The permeability ratio was determined by measuring the reversal potential shift upon replacing total external Cl^- by other anions. All the results in this paper are presented as mean ± SEM.

Single-Channel Recordings

Procedures for obtaining inside-out patches were as previously described (Lin et al., 1999). Except where indicated, the pipette (extracellular) solution was (mM): 110 NMDG-Cl, 5 $MgCl_2$, 1 $CaCl_2$, 5 HEPES, pH 7.6. The bath (intracellular) solution contained (mM): 110 NaCl, 5 $MgCl_2$, 1 EGTA, 5 HEPES, pH 7.6. The current, filtered at 200 Hz (−3 dB corner frequency, four-pole

[1]*Abbreviations used in this paper:* MTS, methanethiosulfonate; MTSEA, 2-aminoethyl MTS; MTSES, 2-sulphonatoethyl MTS; MTSET, 2-(trimethylammonium)ethyl MTS; MTSPA, 3-aminopropyl MTS.

Bessel), was digitized by an acquisition board (DAP 800; Microstar) at 1 kHz with home-made software (Chen and Miller, 1996; Lin et al., 1999). In the SCN^- blocking experiments (see Fig. 3, C and D), both sides of the membrane patch have the same solution containing (mM): 110 NMDG-Cl, 5 $MgCl_2$, 1 EGTA, 5 HEPES, pH 7.6, with the indicated concentrations of NaSCN being added to the pipette solution. The presence of Na^+ or $NMDG^+$ on either side of the membrane did not significantly affect the single-channel conductance or the gating properties.

To analyze a two-pore channel (see Fig. 6, A and B), the absolute open probability of the channel (average of two pores) was determined from the probabilities of three equally spaced conductance levels, D (down), M (middle), and U (upper) (Eq. 1):

$$P_o = f_M/2 + f_U, \tag{1}$$

where f_M and f_U were the measured probabilities at the M and U levels, respectively. When only two levels were present, as in the one-pore channel, P_o was determined, after inactivation events were removed, as the probability of the open level.

To examine the state probabilities of the three conductance levels in the heterodimer (see Fig. 6 D), the expected state probabilities of the D, M, and U levels were calculated according to two different models. In one, a binomial distribution was assumed and the predicted probabilities of the three current levels were:

$$f_0 = (1 - P_o)^2, \tag{2a}$$

$$f_1 = 2P_o(1 - P_o), \tag{2b}$$

and

$$f_2 = P_o^2, \tag{2c}$$

where P_o was the average open probability of the channel obtained from the P_o-V curve of the heterodimer. In the other model, the two pores were assumed to have different fast-gate open probabilities, and the expected probabilities of the three current levels follow a multinomial distribution:

$$f_0 = (1 - P_a)(1 - P_b), \tag{3a}$$

$$f_1 = P_a + P_b - 2P_aP_b, \tag{3b}$$

and

$$f_2 = P_aP_b, \tag{3c}$$

where P_a and P_b are the measured open probabilities obtained from the P_o-V curves of the K165 and K165C* homodimers, respectively. The expected values, f_0, f_1, and f_2, were then compared with the experimental values, f_D, f_M, and f_U, as shown in Fig. 6 D (below).

Comparison of MTSEA Modification Rates

The MTSEA modification rate was examined with pulsing protocol 2 at 0.5 Hz. Because the induced current was measured at +40 mV where the fast gate opens completely ($P_o \cong 1$) in both the homo- and heterodimers, the apparent current induction rate is not influenced by the fast-gate open probability. On the other hand, the current induction rate is affected by the slow-gate open probability of the channel. Fig. 9 A (below) depicts two schemes for the MTSEA modifications in the homodimeric and heterodimeric channels. In low concentrations of MTSEA, the reaction schemes can be further reduced to linear models with two (S_1 and S_2 in the heterodimer) and three (D_0, D_1 and D_2 in the homodimer) states, where S and D represent single and double cysteine mutations and the subscripts denote the number of the open pores. Let α and β be the slow-gating transition rates, λ and μ the pseudo-first-order on and off rate for K165C modification, and P_{S1}, P_{S2}, P_{D1}, and P_{D2} the slow-gate open probabilities of S_1, S_2, D_1, and D_2 states, respectively. When μ is small, the normalized current-induction time courses of the heterodimeric and homodimeric channels are approximated by Eqs. 4 and 5:

$$I_S(t) = 1 - (1 - 0.5\,P_{S1}/P_{S2})e^{-\lambda t} \tag{4}$$

and

$$I_D(t) = 1 + (1 - P_{D1}/P_{D2})e^{-2\lambda t} - (2 - P_{D1}/P_{D2})e^{-\lambda t}. \tag{5}$$

Theoretical curves were thus generated assuming $P_{S1} = P_{D1}$ and $P_{S2} = P_{D2} = 1$ (see Fig. 9 B, left). The curves were fitted to single-exponential functions and the ratios of the fitted time constants were plotted against P_{D1}/P_{D2} (see Fig. 9 B, right). Experimentally, the modification rates were examined in ND96 containing 1–10 μM MTSEA (see Fig. 9 C) with a bath solution exchange time constant of ~3 s. Current amplitudes were measured at the end of the +40-mV voltage step and data points were fitted to single-exponential functions.

RESULTS

Functional Recovery of the Cysteine Mutant with MTSEA Modification

The residue K231 in ClC-1 was suggested to be within the pore (Fahlke et al., 1997b) and, when replaced with a cysteine residue, the mutant K231C was functional and susceptible to inhibition by MTS reagents (Fahlke et al., 1998). Replacing the corresponding residue in ClC-0, K165, with a cysteine residue in the background of the wild-type channel (K165C/wt) did not result in functional channels. We attempted to activate dormant K165C channels by reacting the channels with MTSEA, which converts the side chain of cysteine to a lysine-like side chain. These attempts met with only sporadic success. However, robust MTSEA-activation of K165C channels was observed when we used as genetic background the inactivation-suppressed C212S construct. C212S has the same single-channel conductance and fast-gating properties as those of wild-type ClC-0, but inactivation in this point mutant is undetectable (Lin et al., 1999). As will be shown later, the gating behaviors of the MTSEA-modified K165C channel is better defined in the background of C212S mutation. Therefore, all the following studies were performed on channels with background C212S mutation.

An example of current induction of K165C by MTSEA is shown in Fig. 1 A. Upon the application of MTSEA in the bath solution, ClC-0-like current can be induced. This MTSEA-induced current can be reversed

slowly by washing out the modifying reagent, with a current reduction time constant of ~30 min at ~20°C (Fig. 1 B). A reducing reagent, dithiothreitol, speeded up this reversing process (Fig. 1 A), indicating that the effect was through a sulfhydryl group. The modification was specific to the introduced cysteine because MTSEA had no effect on wild-type ClC-0 or C212S (data not shown). Another two MTS reagents, 2-(trimethylammonium)ethyl MTS (MTSET) and 2-sulphonatoethyl MTS (MTSES) (Akabas et al., 1992; Stauffer and Karlin, 1994), did not induce current, but both compounds blocked the effect of MTSEA (Fig. 1 D). Therefore, these two reagents can also modify the introduced cysteine without generating functional channels. We have also used 3-aminopropyl MTS (MTSPA) to modify the channel. This attaches a slightly longer side chain to cysteine than that of MTSEA modification (see Fig. 1 C for the side-chain structures after modifications by MTS reagents), and MTSPA can also induce current in the K165C mutant (Fig. 1 E).

Gating Properties of the MTSEA-modified Homodimer

Modification of cysteine by MTSEA converts the side chain to a structure similar to that of a lysine residue (Fig. 1 C), presumably the reason for the reopening of the channel. We thus adopt the name K165C* for the MTSEA-induced functional homodimeric channel with C* representing the MTSEA-modified cysteine. The fast gating of K165C* was similar to that of the wild-type

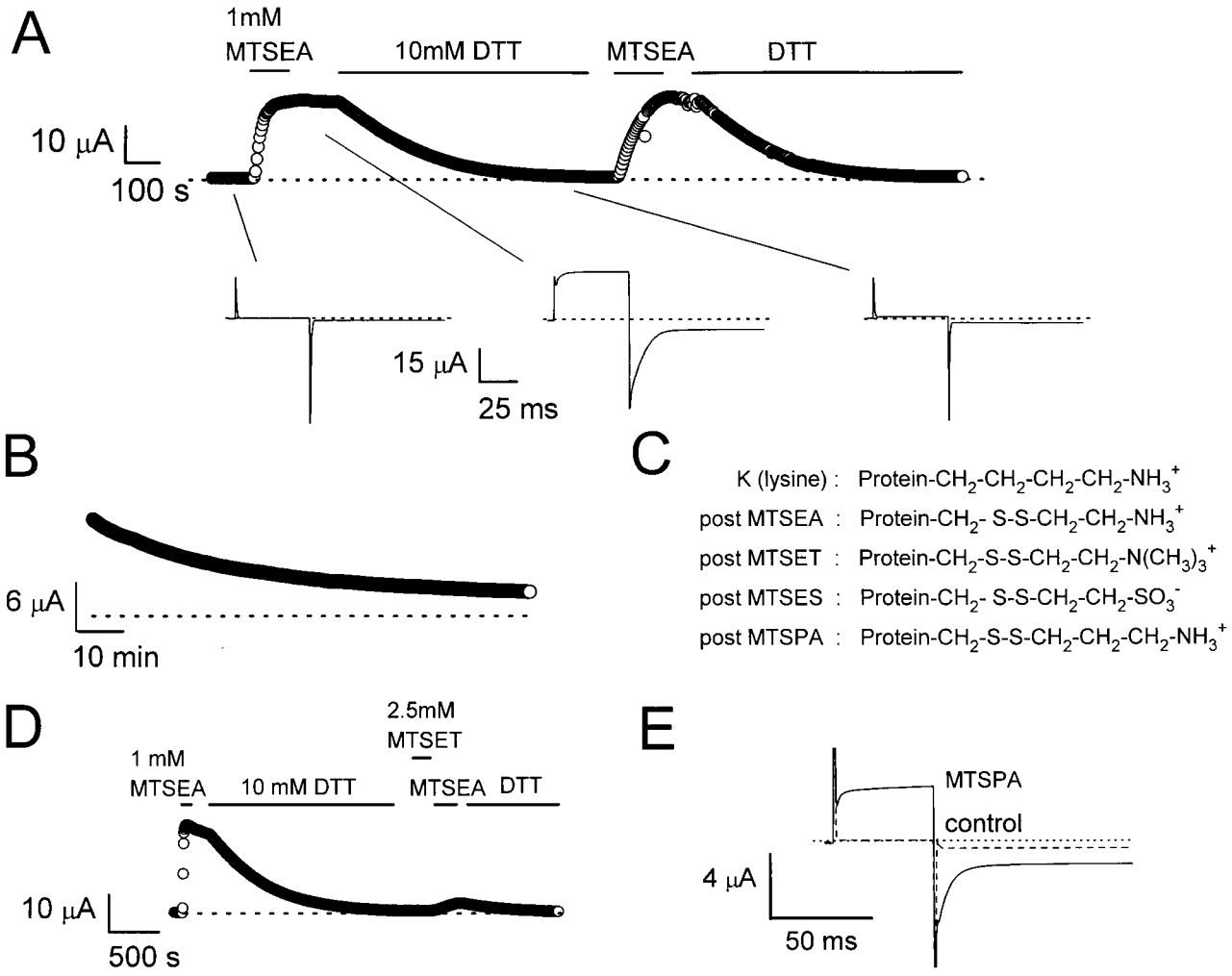

FIGURE 1. Modification by MTS reagents of K165C/C212S channels expressed in *Xenopus* oocytes. (A) Functional current induced by MTSEA. Repeated pulsing protocol 2, given one pulse every 2 s. Reagents applied as indicated by horizontal lines. (○) Current amplitudes measured at +40 mV. Examples of the current traces before and after MTSEA, and finally after dithiothreitol treatment are shown. Dotted lines are zero-current level. (B) Reduction of MTSEA-induced current after washout of the modifying reagent. Repeated pulsing protocol 1. Temperature, 20°C. (C) Side-chain structure of lysine and those of cysteine modified with various MTS reagents. (D) Modification of K165C by MTSET without generating functional channels. Pulsing protocol 1 used in this experiment. MTSES produced similar effects in blocking the current induction by MTSEA (data not shown). (E) Current induction in K165C channel by MTSPA. Dashed and solid curves represent the average of three recording traces before (control) and after the application of 0.2 mM MTSPA. Dotted line is zero-current level.

channel containing lysine at the 165 position, with current deactivation at −150 mV (Fig. 1 A). However, the P_o-V curve of K165C* was right shifted by 45 mV when compared with that of the K165 channel at an external Cl^- concentration ($[Cl^-]_o$) of ~100 mM (Fig. 2 A). This curve was further shifted towards a more depolarized membrane potential in response to a low $[Cl^-]_o$. The $V_{1/2}$ of the P_o-V curves in both channels had a more negative value at higher $[Cl^-]_o$, but the effect was saturated at $[Cl^-]_o > 150$–300 mM. Furthermore, there was always an ~40–50-mV difference in $V_{1/2}$ between two channels at the same $[Cl^-]_o$ (Fig. 2 B). This difference was mostly due to a shift of the opening rate curve of K165C* towards a more depolarized membrane potential (Fig. 2 C), an effect similar to that of lowering $[Cl^-]_o$ on the wild-type channel (Pusch et al., 1995; Chen and Miller, 1996). Since the ability of external Cl^- to shift the fast-gate P_o-V curve is mediated by the Cl^--binding sites in the pore, we analyzed the $[Cl^-]_o$ dependence of the fast-gate opening rate derived from macroscopic current recordings (Fig. 2 D). Curve fitting to hyperbolic equations suggested that the apparent affinity for Cl^- binding (Chen and Miller, 1996) was not changed. Rather, the effect may result from a higher energy barrier in the subsequent Cl^- translocation process that drives the bound Cl^- to open the channel (Chen and Miller, 1996). In addition to the fast-gating properties, we also examined the slow gating of K165C*. Both

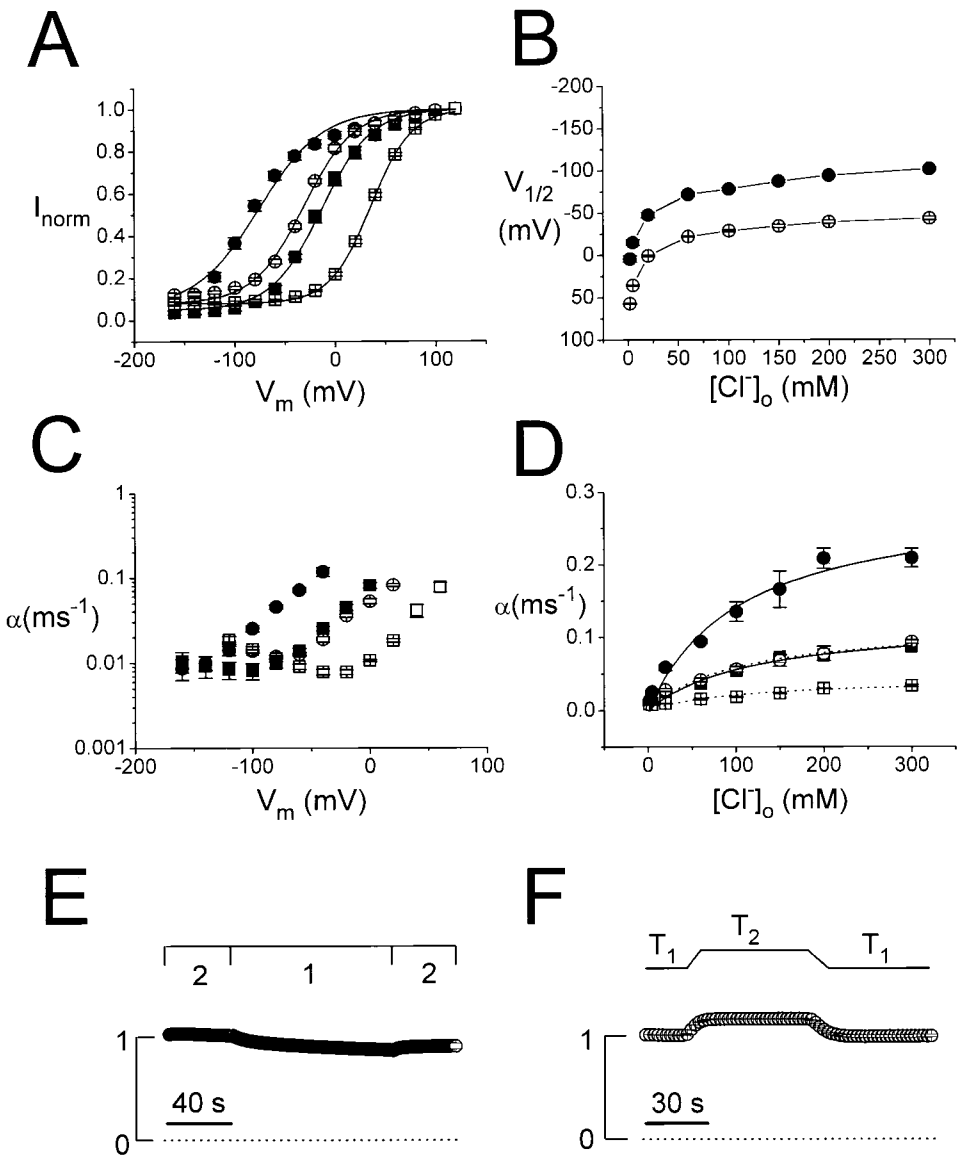

FIGURE 2. Fast- and slow-gating properties of K165 (filled symbols) and K165C* channels (open symbols) derived from macroscopic current recordings. (A) Comparison of the fast-gate P_o-V curves at 100.6 (circles) and 4.6 mM (squares) of $[Cl^-]_o$. Solid curves were drawn according to a Boltzmann equation: $P_o = P_{min} + (1 - P_{min})/\{1 + \exp[-zF(V - V_{1/2})/RT]\}$, with z = 0.8–1.2, P_{min} = 0.05–0.08. $V_{1/2}$s in 100.6 and 4.6 mM $[Cl^-]_o$ were: (K165) −76 and −14 mV; (K165C*) −31 and 35 mV. (B) $V_{1/2}$s of the fast-gate P_o-V curves as a function of $[Cl^-]_o$ (n = 3–8). (C) Opening rates, α, of the fast gate for K165 and K165C* channels in 100.6 and 4.6 mM $[Cl^-]_o$. Symbols are the same as in A (n = 3–8). (D) Opening rates of the channels as a function of $[Cl^-]_o$. Data points taken at −40 (●) and −80 mV (■) for the K165 channel and at 0 (○) and −40 mV (□) for the K165C* channel. Solid and dotted curves were the best fit to the hyperbolic equation, $\alpha = \alpha_{max}[Cl^-]_o/(K_{1/2} + [Cl^-]_o)$. The fitted α_{max}s are (ms^{-1}): K165, 0.29 (−40 mV) and 0.12 (−80 mV); K165C*, 0.12 (0 mV) and 0.04 (−40 mV). The fitted $K_{1/2}$s are (mM): K165, 107 (−40 mV) and 121 (−80 mV); K165C*, 103 (0 mV) and 108 (−40 mV). (E) Slow-gating transition examined by voltage activation. 30–40 μM MTSEA in the bath solution. Numbers 1 and 2 are the pulsing protocols (see MATERIALS AND METHODS) used in the indicated periods (n = 3). Current amplitudes normalized to that of the point right before pulsing protocol 1. Dotted line represents zero-current level. (F) Temperature jump experiment revealed that the probability of closing the slow gate was only minimal upon raising the bath temperature. Pulsing protocol 1. 30–40 μM MTSEA was present. Current amplitudes normalized to that of the first point. T_1 = 21.4°C, T_2 = 27.5°C (n = 3).

the voltage (Fig. 2 E) and temperature (F) changes resulted in almost no change in the open probability of the slow gate, a phenomenon most likely resulting from the C212S mutation (Lin et al., 1999). As will be shown later, the little inactivation in this channel provides a well defined slow-gating behavior that is important in interpreting the apparent MTS modification rate.

K165 Is Likely to be Located in the Pore Region

As the shift of the P_o-V curve was thought to be a pore property, we suspected that K165 may be located in the pore region. To address this possibility more directly, we compared pore properties between K165 and K165C* channels. The blockage by thiocyanate (SCN^-), a pore blocker of ClC-0 (White and Miller, 1981), was observed in both channels. For the K165 channel, it took 5.5 mM external SCN^- to block half of the current at +40 mV, but only 1.3 mM SCN^- was needed to reach the same effect in the K165C* channel (Fig. 3, A and B). Examination of the effect of SCN^- on single-channel conductance corroborates the apparent blocking affinities derived from macroscopic current recordings in both channels (Fig. 3, C and D), suggesting that K165 is likely to be located near the pore. Another piece of evidence to support the pore location of K165 comes from a reduction in the channel conductance when K165C was modified by MTSPA. In both the K165C homodimer (Fig. 4 A) and K165C-K165 heterodimer (B), the channel conductance of the MTSPA-modified pore was ~50–60% of that of the wild-type or the MTSEA-modified pore (also see results below). In addition, the MTSPA-modified pores have the same conductance irrespective of the side chain at residue 165 in the other subunit, an observation favoring two independent pores. The MTSPA-modified cysteine has a side chain slightly longer than the MTSEA-modified side chain (Fig. 1 C), a subtle change that influences the rate of Cl^- permeation. We have also compared the permeation of various anions in the K165 and K165C* channels. Both channels revealed an anomalous mole fraction effect for mixtures of Cl^- and SCN^- with a difference in the left arms of the normalized curves (Fig. 5), reflecting different SCN^- blocking affinities in these two channels. The anion permeability sequence was $SCN^- > Cl^- > Br^- > NO_3^- > I^-$ for both channels (permeability ratios: K165, 1.20 ± 0.04:1:0.80 ± 0.02:0.66 ± 0.02:0.44 ± 0.04, n = 5; K165C*, 1.22 ± 0.08:1:0.95 ± 0.03:0.74 ± 0.02:0.51 ± 0.05, n = 3–5). The small alteration in ion permeation suggests that the K165C* mutation has not altered too much the global structure of the channel pore.

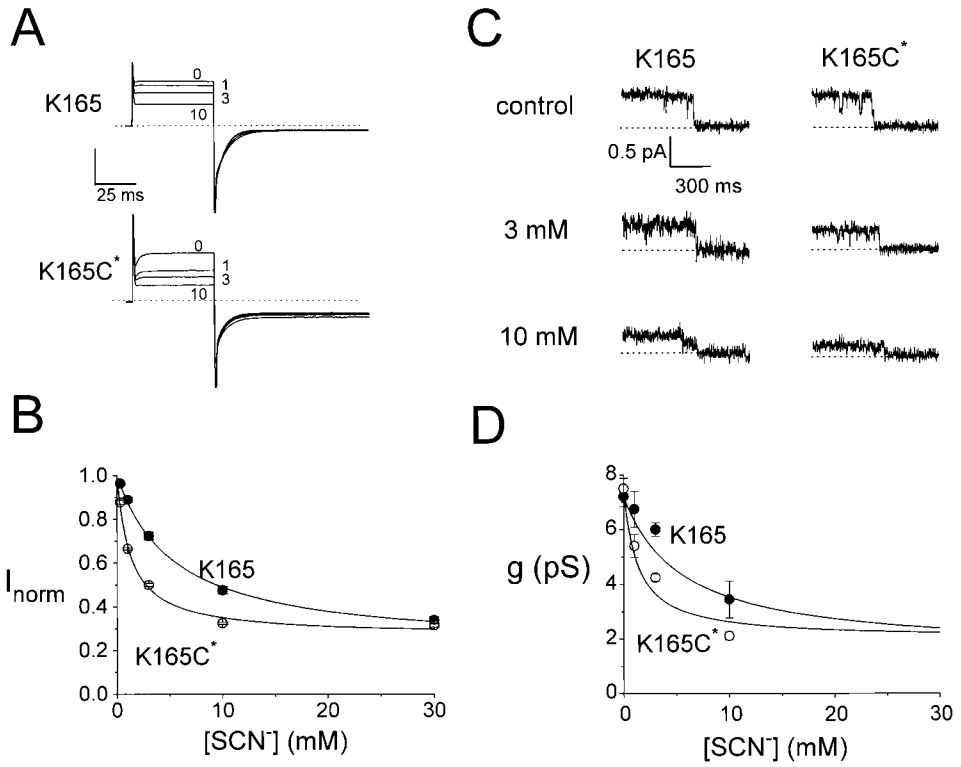

FIGURE 3. Comparison of the SCN^- block between K165 and K165C* channels. (A) SCN^- block of the whole oocyte current. Pulsing protocol 2. Numbers indicate the SCN^- concentrations (millimolar) in the bath solution. Dotted lines are zero-current level. Vertical scale bar represents 12 and 2 μA for K165 and K165C*, respectively. (B) The K165C* channel was more sensitive to the SCN^- block. Data points derived from experiments like those in A. Solid curves were drawn according to: $I_{norm} = I_\infty + (1 - I_\infty)/(1 + [SCN^-]/K_{1/2})$, with values of $K_{1/2}$ and I_∞: (K165) 5.5 mM and 0.21; (K165C*) 1.3 mM and 0.27 (n = 4). (C) Single-channel recording of the SCN^--blocked K165 and K165C* channels at +40 mV. Symmetrical solutions on both sides of the membrane except that the indicated concentrations of NaSCN were added in the pipette solution. Dotted lines are zero-current level. (D) Averaged single-pore conductance at +40 mV (n = 3–8). The two current levels in traces like those shown in C were determined from all-points amplitude histograms and the difference in current was divided by two to calculate the conductance of one pore. Solid curves are the same curves from B after multiplying the respective channel conductance in the absence of SCN^-.

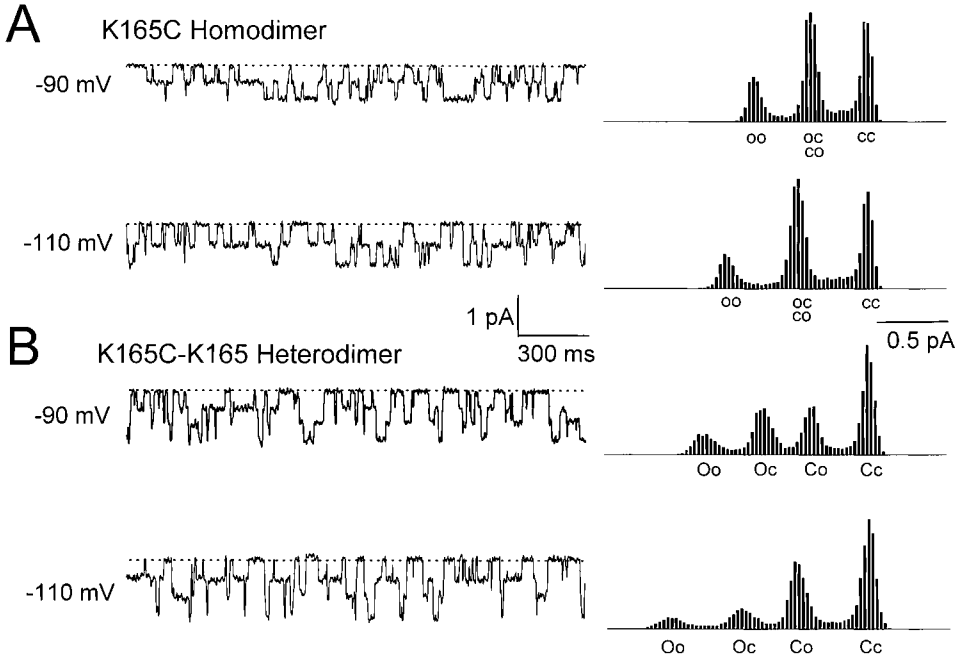

FIGURE 4. (A) Single-channel recordings of the MTSPA-modified K165C homodimer at −90 and −110 mV. Dotted lines represent zero-current level. Next to each trace are current amplitude histograms compiled from 30 s (top and bottom) of recording traces containing the 2-s examples on the left. (B) Single-channel recordings of the MTSPA-modified K165C-K165 heterodimer. Amplitude histograms were from 23 s (top) and 30 s (bottom) of recording traces. Capital and small letters represent the pores with big and small conductances, respectively. C, close; O, open. The smaller conductance level in the heterodimer corresponds to the MTSPA-modified pore and is equal to the conductance levels in the homodimer shown in A.

Fast Gating of Heterodimeric Channels Revealed Double-Barrel–like Behaviors

With tandem heterodimers containing K165 in one subunit and K165C in the other, the functional role of K165 in ClC-0 gating can be further characterized. The MTSEA-modified tandem heterodimers revealed a double-barrel–like structure, as with K165 or K165C* homodimers (Fig. 6 A). The average P_o of the two pores in either configurations (K165C*-K165 or K165-K165C*) was close to the mean of those of the K165 and K165C* homodimers (Fig. 6 B). However, the P_o of each individual pore was different from that of the other pore. For example, the probabilities of the three current levels showed a multinomial distribution when the P_o of one pore was equal to the P_o of K165 and the other to that of K165C* channels (Fig. 6, C and D). Furthermore, when recording single MTSEA-modified heterodimeric channels, we frequently observed a transition from three to two current levels, presumably due to the loss of the modifying group. Subsequent examination of such a two-level trace always revealed a P_o close to that of the K165 channel (Fig. 7). These results together indicate that the two pores of the MTSEA-modified heterodimer have equal conductance and different P_o; nevertheless, the principle of independent gating is still preserved.

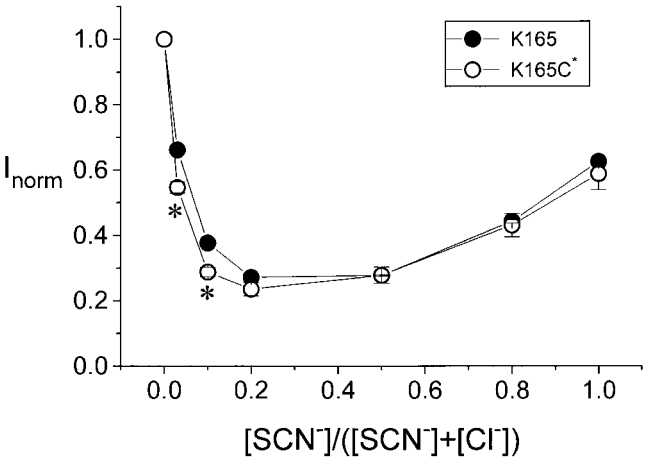

FIGURE 5. Comparison of the anomalous mole fraction effect for mixtures of Cl^- and SCN^-. All measured currents were normalized to the current obtained in the absence of NaSCN. Each point represents the average of four measurements. *Significantly different ($P < 0.05$, Student's t test) from the K165 channel.

One-Pore Channel Is Easier to Inactivate

The independence shown above for the fast gating, however, was not observed with respect to inactivation because the latter is influenced by both pores (Ludewig et al., 1996). Without MTSEA, the tandem heterodimer revealed only two current levels with prominent inactivation events (Fig. 8 A), even though the mutation was constructed in the background of C212S. The inactivation process in this one-pore channel was both voltage and temperature dependent (Fig. 8, B and C). With MTSEA modification, the second pore became functional and the open probability of the slow gate of the two-pore channel was greatly increased (Fig. 8, D–F) to a probability similar to that of the K165C* homodimer (Fig. 2, E and F). These results indicate that residue K165 is also important in the slow gating, and the open probability of the slow gate is determined by both pores. The closure of one pore renders the channel

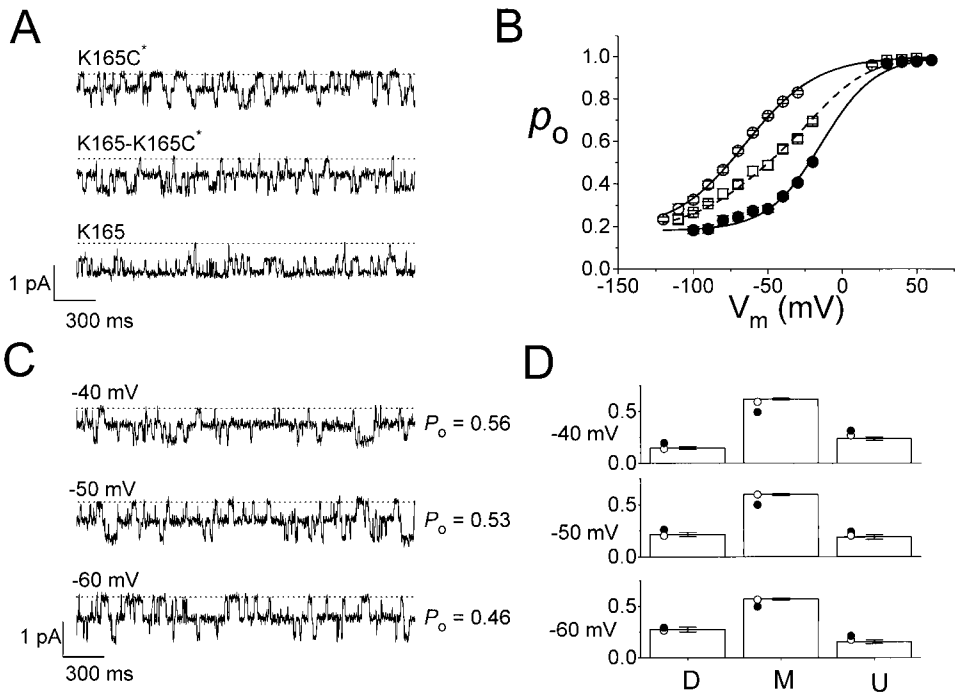

FIGURE 6. Fast-gating properties of heterodimers after MTSEA modification. (A) Single-channel recording traces of K165C*, K165-K165C*, and K165 channels. Membrane potential, −40 mV. Dotted lines are zero-current level. (B) P_o-V curves derived from single-channel recordings (n = 3–7). Solid curves are Boltzmann curves for K165 (○) and K165C* (●) channels, while the dashed curve is simply the average of the two solid curves. (□) The measured P_o of the heterodimers (average of K165-K165C* and K165C*-K165). (C) Single-channel recordings of the heterodimer K165C*-K165 at three different voltages. Open probabilities shown on the right were calculated from >40-s continuous recordings, including the three traces shown at left. (D) Comparison of the measured state probabilities (bars) with the expected state probabilities (circles). (●) Calculated from the averaged P_o of the heterodimer according to Eqs. 2a–2c (binomial distribution). (○) Calculated according to Eqs. 3a–3c, assuming distinct P_o's for two pores (multinomial distribution). The open probabilities were taken from the P_o's of the homodimers at the corresponding voltages shown in B. Statistical analysis showed significant difference ($P < 0.01$, one sample t test, SPSS 8.0; SPSS, Inc.) between the measured probabilities of the M level and the expected values derived from the binomial model in all three voltages. The comparisons of the measured probabilities with the expected values from the multinomial model, however, showed no difference ($P > 0.01$).

easier to inactivate, recapitulating the previously reported nonequilibrium gating cycle of ClC-0 (Richard and Miller, 1990).

Independent Modification of the Two Introduced Cysteine Residues in a Homodimer

Complete modification of a homodimeric K165C channel requires two steps and must go through the low slow-gate open probability, one-pore state. Thus, the current-induction rate in the homodimer cannot be identical with that in the heterodimer. Fig. 9 A shows possible schemes for MTSEA reaction with the hetero- and homodimeric channels. We assume that each cysteine residue is modified independently and the reaction rates in the inactivated and noninactivated channels are the same. When the on rate (λ) of MTSEA modification is slower than the slow-gating transition rates (α and β), but much faster than the off rate (μ), the reaction schemes can, respectively, be reduced to a two- (S_1 and S_2) and a three- (D_0, D_1, and D_2) state model. When each state X has a slow-gate open probability P_X, calculations show that the apparent modification rate would be slower in the homodimer than in the heterodimer as long as $P_{D1} < P_{D2}$ (Fig. 9 B). Experimentally, we applied 1–10 μM MTSEA to induce the current with time constants in the range of ~20–200 s (Fig. 9 C, left). The ratios of the time constants for current induction in the homodimer compared with those in the heterodimer ranged from 1.4 to 1.7 (Fig. 9 C, right), a result close to the expected ratio if the one-pore channel has a low open probability for the slow gate (B). This result indicates that the two cysteine residues reacted with MTSEA independently and the difference in the apparent modification rate was due to the distinct open probabilities of the slow gate in the one- and two-pore channels.

DISCUSSION

Evidence for a Possible Pore Location of K165

We have found that residue K165 plays important roles in gating and permeation properties of ClC-0. The residue is freely accessible to all external MTS reagents tested. Therefore, K165 in ClC-0 is located at the extracellular side, consistent with both topological models proposed previously (Fahlke et al., 1997a,b; Schmidt-Rose and Jentsch, 1997). The K165C channel could be functionally recovered after modification of the introduced cysteine by MTSEA or MTSPA but not by MTSET or MTSES, indicating that the charge at position 165 is not the only determining factor for a functional channel. After modification by MTSEA, the K165C* channel shows distinct gating properties from those of the wild-

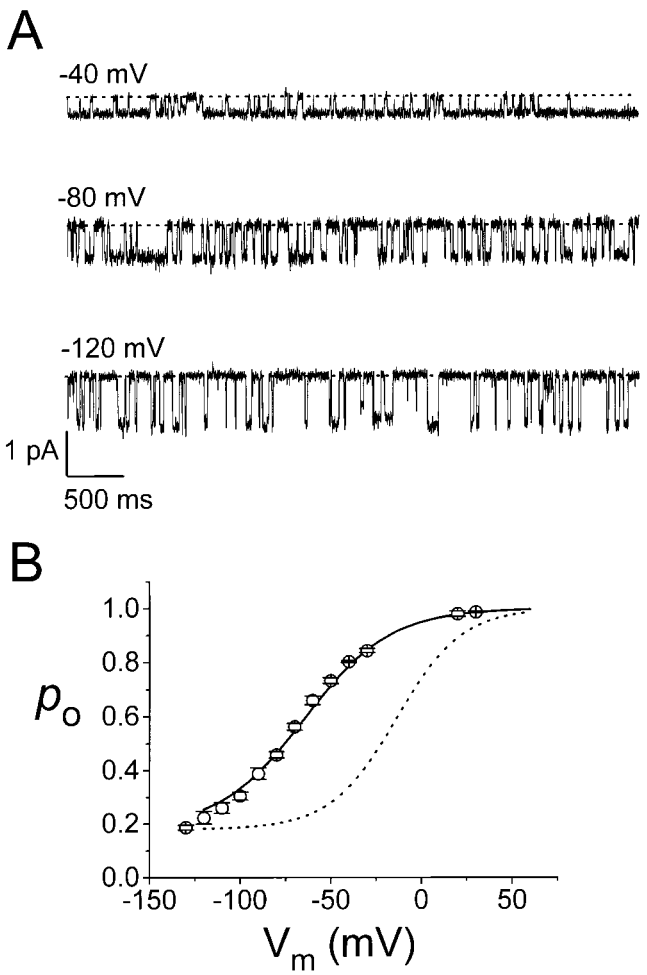

FIGURE 7. Fast gating of the heterodimer without MTSEA modification. (A) Single-channel recording traces of the heterodimer K165C-K165 at different voltages. Dotted lines represent zero-current level. (B) Steady state P_o-V curve of the single-pore heterodimer. (○) The average of three to eight measurements from traces like those shown in A. Solid and dotted curves are the same Boltzmann curves for the K165 and K165C* homodimers, respectively, as those shown in Fig. 6 B.

type K165 channels. The fast-gate P_o-V curve of the K165C* channel shifted in parallel to more depolarized potential by ~45 mV, an effect similar to that of $[Cl^-]_o$ reduction. The shift of the fast-gate P_o-V curve of ClC-0 upon reducing $[Cl^-]_o$ has been suggested to be mediated by chloride binding sites in the pore (Pusch et al., 1995; Chen and Miller, 1996). We therefore searched for a possibility that the residue K165 may be located in or near the outer pore region. External SCN^- blocking experiments indicated that the K165C* and K165 pores showed an approximately fourfold difference in the affinity for this pore blocker (Fig. 3). In addition, a change in the single-channel conductance was observed in the MTSPA-modified K165C pore (Fig. 4). These two results suggest that K165 residue is likely to be located in the external pore region.

MTS Modifications of K165C Support the Double-Barrel Model

The shift of the fast-gate P_o-V curve of the K165C* channel also provides a chance to examine the pore stoichiometry in this channel. When analyzing the fast gating of the heterodimers, we found that a multinomial distribution describes gating among the three current levels, with the P_o of individual fast gates corresponding to those of the K165 and K165C* pores (Fig. 6 D). Furthermore, the channel without MTSEA modification showed only one pore, and the P_o was similar to that of the K165 homodimer (Fig. 7). These results are all consistent with a picture of two independent fast gates. In addition, both the MTSPA- and MTSEA-modified channels revealed that the conductances of the two pores are independent of each other; that is, irrespective of the side chain of residue 165 in the other subunit (Figs. 4 and 6 A). This result further supports the two-pore picture. Fahlke et al. (1998) argued previously that the ClC channel may contain only one pore and the side chains of the two residues from different subunits may coordinate in a way so that conformational changes in the single pore may mimic the behavior of multiple ion-conduction pathways. However, with independent modifications in ClC-0 occurring on the two internal K519C's (Middleton et al., 1996) and on the two external K165C's (this study), it is very difficult to devise a one-pore model to accommodate the independent modifications on both sides of the membrane. The K165C modification shown in the present study does not support the notion that the two K165's reside in a shared outer vestibule connected by the two protopores. We therefore still conclude that a functional ClC-0 channel contains two separate ion-conducting pathways.

Gating Effects of MTS Modification Invalidate the Assumption Used to Compare the MTS Inhibition Rates in ClC-1

One of the experiments supporting the one-pore conclusion in ClC-1 was a comparison of the MTS modification rates between the homo- and heterodimers. In this experiment on ClC-1, a key assumption was that the MTS inhibition of the channel is due to pore occlusion and thus the modification rates of the homo- and heterodimers should be the same if the channel has two pores (Fahlke et al., 1998). This assumption is false even though the residue K165 (or K231 in ClC-1) appears to be located near the entrance to the pore. In addition to an effect on ion permeation, our experimental evidence revealed that MTSEA modification also influences the fast and slow gating of the channel. The gating effect of MTS reagents prompts several cautions. First, because even a slight change of the side chain at residue 165 (for example, K165 vs. K165C*) leads to an ~45-mV shift in the P_o-V curve, it is important to monitor the MTSEA-induced current at a mem-

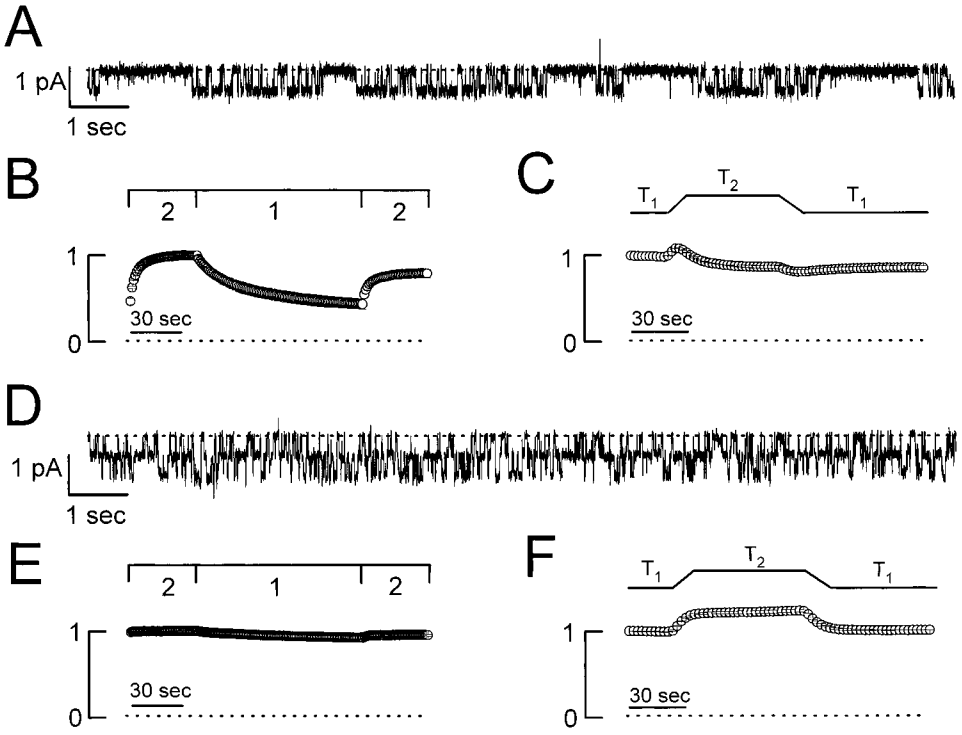

FIGURE 8. Slow-gating behaviors of the heterodimer. (A–C) Slow gating of the heterodimer without MTSEA modification. (A) Single-channel trace at −60 mV revealed two current levels and several short inactivation events. (B) Voltage activation experiment to examine slow-gating transitions at the macroscopic current level ($n = 3$). (C) Temperature-jump experiment revealed prominent inactivation relaxation ($n = 3$). $T_1 = 22.5°C$, $T_2 = 28.2°C$. Symbols and experimental procedures for B and C were as in Fig. 2, E and F. (D–F) Slow-gating behaviors of the MTSEA-modified heterodimers. (D) Single-channel recording of a MTSEA-modified heterodimer. Membrane potential, −60 mV. (E and F) Voltage and temperature jump experiments ($n = 3$). Procedures were as in B and C with 30–40 μM MTSEA in the bath. $T_1 = 21.9°C$, $T_2 = 28.1°C$.

brane potential where the fast-gate open probabilities of the homo- and heterodimers are the same. We achieved this requirement by monitoring the MTSEA-induced current at +40 mV, where the fast-gate open probabilities of the homo- and heterodimers are both close to unity (Fig. 6 B).

A second point to be considered in comparing the apparent MTS modification rates concerns the slow gating of the channel. Our results showed that the channel with only one functional pore was easier to inactivate than the two-pore channel (Fig. 8). This is consistent with a previous observation on the single-channel behaviors that the channel inactivates from the middle level and recovers from the inactivation state into the upper level more frequently (Richard and Miller, 1990). We do not understand the underlying molecular mechanism, but this property demands that the K165C homodimer acquire two states with unequal slow-gating behaviors in the process of MTSEA modification. The singly modified channel, with only one functional pore, must have a lower slow-gate open probability than the fully modified channel. This will lead to a slower apparent current induction in the homodimer than in the heterodimer, as revealed by the theoretical calculations (Fig. 9 B). Experimental comparison of the modification rates between these two channels indeed showed that this is the case (Fig. 9 C).

The third caution in the interpretation of MTS modification rates concerns the concentrations of the modifying reagents. The MTS modification schemes (Fig. 9 A, top) can be reduced to linear schemes only when the modification rate is much slower than the slow-gating transition rate. In our experiments, we used very low concentrations of MTSEA (1–10 μM) to fulfill this condition. Under such circumstances, the time courses of current induction were typically 2–10-fold longer than that of the slow-gating relaxation of the heterodimer. We are therefore confident that the apparent current-induction rates mostly reflect the true MTSEA modification rates on the introduced cysteine residues. On the other hand, if the true modification rate were faster than the slow-gating transition rate, the apparent rate would mostly reflect the gating transition rate of the channel.

It is not known at this stage which of the above reasons contributes most to the different apparent modification rates between the homo- and heterodimers of ClC-1 because characterization of the MTS effects on channel gating has not been performed in this muscle channel. However, the K231C homo- and heterodimers of ClC-1 showed very distinct gating behaviors from those of the wild-type channel (Fahlke et al., 1998), indicating that this residue is also important in ClC-1 gating. Clearly, there are differences in gating properties between ClC-0 and ClC-1 because the lysine-to-cysteine mutations in the corresponding positions (K165 in ClC-0 and K231 in ClC-1) result in nonfunctional and functional channels, respectively. However, due to the importance of this residue in channel gating, the inhibitory effects of MTS reagents on the K231C mutant of

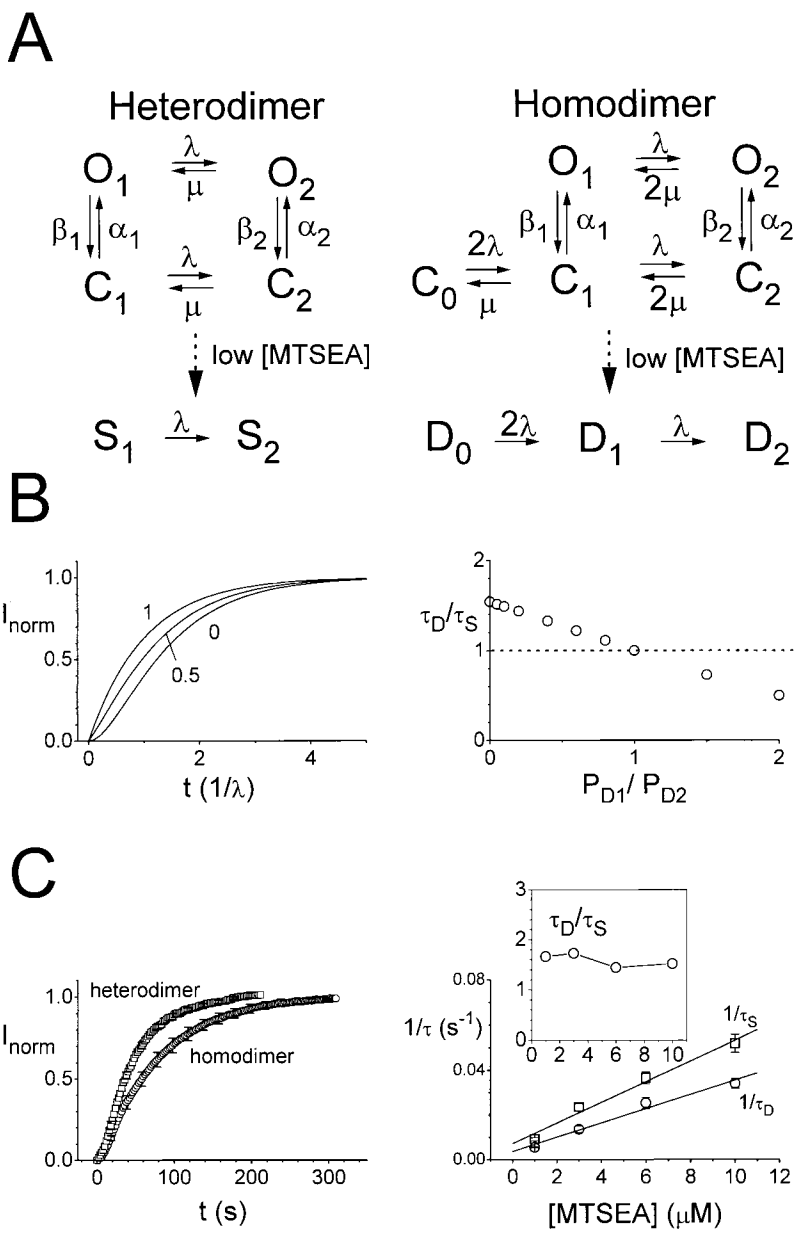

FIGURE 9. Independence of MTSEA modification on the introduced cysteines. (A) Reaction schemes for MTSEA modification. When the modification rates are smaller than the slow-gating transition rates, the schemes can be reduced to linear models. (B) Slow-gate open probability contributes to the apparent MTSEA-modification rate. (Left) Calculated current-induction curves of the homodimer (Eq. 5) when P_{D1}/P_{D2} are 0, 0.5, and 1, respectively. The normalized curve of the heterodimer (Eq. 4) is the same as that of the homodimer when $P_{D1}/P_{D2} = 1$. (Right) Ratios of the time constants derived from single-exponential curve fittings plotted against P_{D1}/P_{D2}. (C) Experimental comparison of the apparent modification rates between hetero- and homodimeric channels. (Left) Current induction in the heterodimer (□, $n = 6$) and homodimer (○, $n = 3$) by 3 μM MTSEA. All current amplitudes, after subtraction by the current before applying MTSEA, were normalized to the maximal current induced by MTSEA. One error bar plotted in every 10 points. Time constants were 49.3 and 80.7 s for the hetero- and homodimer, respectively. (Right) Current-induction rates in the homodimeric (○) and heterodimeric channels (□) at various concentrations of MTSEA. The slopes and y intercepts of the solid lines were: (heterodimer) 7.2×10^3 $M^{-1}s^{-1}$ and 0.0037 s^{-1}; (homodimer) 4.6×10^3 $M^{-1}s^{-1}$ and 0.0032 s^{-1}. (Inset) Ratios of the induction time constants of the homodimer to those of the heterodimer.

ClC-1 should not be attributed solely to the occlusion of the channel pore (Fahlke et al., 1998).

Unsettled Inconsistency between the Cu^{2+}-Phenanthroline Effect in ClC-1 and the Double-Barrel Conclusion in ClC-0

In ClC-1, the vicinity of K231 in D4 and the end of D5 have been proposed to form the outer vestibule of the pore (Fahlke et al., 1997b; but see Schmidt-Rose and Jentsch, 1997, for a different membrane topology), and the residue K231 was hypothesized to form the selectivity filter. It was also shown that Cu^{2+}-phenanthroline can inhibit the K231C-K231C homodimer, but not the K231C-K231A heterodimer, a result taken to suggest a disulfide-bond formation between the two K231C residues (Fahlke et al., 1998). If this is indeed the case, the two K231 residues (and by analogy the two K165 residues in ClC-0) must be located very close to the twofold axis of the channel and must electrostatically influence each other. Given the double-barrel conclusion in the present work, it is very surprising that the side-chain charge of residue 165 in one pore does not affect the conductance of the other pore (Figs. 4 and 6 A). It would therefore be important to examine the possibility of a disulfide-bond formation between the two K165C residues in ClC-0 to further understand the pore structure of ClC channels.

We thank Dr. M. Maduke and Mr. K.H. Hong from Dr. C. Miller's lab for kindly providing us two mother constructs with convenient restriction enzyme cutting sites to make ClC-0 heterodimers. We also thank Drs. T.-C. Hwang and C. Miller for comments on the manuscript and helpful discussions.

This work was supported by grant NHRI-GT-EX89B813C from the National Health Research Institutes in Taiwan.

Submitted: 3 May 2000
Revised: 2 August 2000
Accepted: 22 August 2000

REFERENCES

Akabas, M.H., D.A. Stauffer, M. Xu, and A. Karlin. 1992. Acetylcholine receptor channel structure probed in cysteine-substitution mutants. *Science.* 258:307–310.

Bauer, C.K., K. Steinmeyer, J.R. Schwarz, and T.J. Jentsch. 1991. Completely functional double-barreled chloride channel expressed from a single *Torpedo* cDNA. *Proc. Natl. Acad. Sci. USA.* 88: 11052–11056.

Chen, T.-Y. 1998. Extracellular zinc ion inhibits ClC-0 chloride channels by facilitating slow gating. *J. Gen. Physiol.* 112:715–726.

Chen, T.-Y., and C. Miller. 1996. Nonequilibrium gating and voltage dependence of the ClC-0 Cl^- channel. *J. Gen. Physiol.* 108:237–250.

Fahlke, C., T. Knittle, C.A. Gurnett, K.P. Campbell, and A.L. George, Jr. 1997a. Subunit stoichiometry of human muscle chloride channels. *J. Gen. Physiol.* 109:93–104.

Fahlke, C., T.H. Rhodes, R.R. Desai, and A.L. George, Jr. 1998. Pore stoichiometry of a voltage-gated chloride channel. *Nature.* 394: 687–690.

Fahlke, C., H.T. Yu, C.L. Beck, T.H. Rhodes, and A.L. George, Jr. 1997b. Pore-forming segments in voltage-gated chloride channels. *Nature.* 390:529–532.

Foskett, J.K. 1998. ClC and CFTR chloride channel gating. *Annu. Rev. Physiol.* 60:689–717.

Hanke, W., and C. Miller. 1983. Single chloride channels from *Torpedo* electroplax: activation by protons. *J. Gen. Physiol.* 82:25–45.

Jentsch, T.J., T. Friedrich, A. Schriever, and H. Yamada. 1999. The CLC chloride channel family. *Pflügers Arch.* 437:783–795.

Jentsch, T.J., K. Steinmeyer, and G. Schwarz. 1990. Primary structure of *Torpedo marmorata* chloride channel isolated by expression cloning in *Xenopus* oocytes. *Nature.* 348:510–514.

Lin, Y.-W., C.-W. Lin, and T.-Y Chen. 1999. Elimination of the slow gating of ClC-0 chloride channel by a point mutation. *J. Gen. Physiol.* 114:1–12.

Ludewig, U., M. Pusch, and T.J. Jentsch. 1996. Two physically distinct pores in the dimeric ClC-0 chloride channel. *Nature.* 383: 340–343.

Ludewig, U., M. Pusch, and T.J. Jentsch. 1997. Independent gating of single pores in CLC-0 chloride channels. *Biophys.J.* 73:789–797.

Maduke, M., C. Miller, and J.A. Mindell. 2000. A decade of CLC chloride channels: structure, mechanism, and many unsettled questions. *Annu. Rev. Biophys. Biomol. Struct.* 29:441–448.

Middleton, R.E., D.J. Pheasant, and C. Miller. 1994. Purification, reconstitution, and subunit composition of a voltage-gated chloride channel from *Torpedo* electroplax. *Biochemistry.* 33:13189–13198.

Middleton, R.E., D.J. Pheasant, and C. Miller. 1996. Homodimeric architecture of a ClC-type chloride ion channel. *Nature.* 383:337–340.

Miller, C. 1982. Open-state substructure of single chloride channels from *Torpedo* electroplax. *Phil. Trans. R. Soc. Lond. B Biol. Sci.* 299: 401–411.

Miller, C., and M.M. White. 1984. Dimeric structure of single chloride channels from *Torpedo* electroplax. *Proc. Natl. Acad. Sci. USA.* 81:2772–2775.

Pusch, M., and T.J. Jentsch. 1994. Molecular physiology of voltage-gated chloride channels. *Physiol. Rev.* 74:813–825.

Pusch, M., U. Ludewig, A. Rehfeldt, and T.J. Jentsch. 1995. Gating of the voltage-dependent chloride channel ClC-0 by the permeant anion. *Nature.* 373:527–531.

Pusch, M., K. Steinmeyer, and T.J. Jentsch, 1994. Low single channel conductance of the major skeletal muscle chloride channel, ClC-1. *Biophys. J.* 66:149–152.

Richard, E.A., and C. Miller. 1990. Steady-state coupling of ion-channel conformations to a transmembrane ion gradient. *Science.* 247:1208–1210.

Rychkov, G.Y., M. Pusch, M.L. Roberts, T.J. Jentsch, and A.H. Bretag. 1998. Permeation and block of the skeletal muscle chloride channel, ClC-1, by foreign anions. *J. Gen. Physiol.* 111:653–665.

Saviane, C., F. Conti, and M. Pusch. 1999. The muscle chloride channel ClC-1 has a double-barreled appearance that is differentially affected in dominant and recessive myotonia. *J. Gen. Physiol.* 113:457–467.

Schmidt-Rose, T., and T.J. Jentsch. 1997. Transmembrane topology of a CLC chloride channel. *Proc. Natl. Acad. Sci. USA.* 94:7633–7638.

Stauffer, D.A., and A. Karlin. 1994. Electrostatic potential of acetylcholine binding sites in the nicotinic receptor probed by reactions of binding-site cysteines with charged methanethiosulfonates. *Biochemistry.* 33:6840–6849.

Steinmeyer, K., C. Ortland, and T.J. Jentsch. 1991. Primary structure and functional expression of a developmentally regulated skeletal muscle chloride channel. *Nature.* 354:301–304.

Valverde, M.A. 1999. ClC channels: leaving the dark ages on the verge of a new millennium. *Curr. Opin. Cell Biol.* 11:509–516.

White, M.M., and C. Miller. 1981. Probes of the conduction process of a voltage-gated Cl^- channel from *Torpedo* electroplax. *J. Gen. Physiol.* 78:1–19.